ACS Energy LETTERS

http://pubs.acs.org/journal/aelccp

LETTER

Predicting Charge Transfer Stability between Sulfide Solid Electrolytes and Li Metal Anodes

Haesun Park, Seungho Yu, and Donald J. Siegel*

Cite This: *ACS Energy Lett.* 2021, 6, 150–157

Read Online

ACCESS | Metrics & More | Article Recommendations | Supporting Information

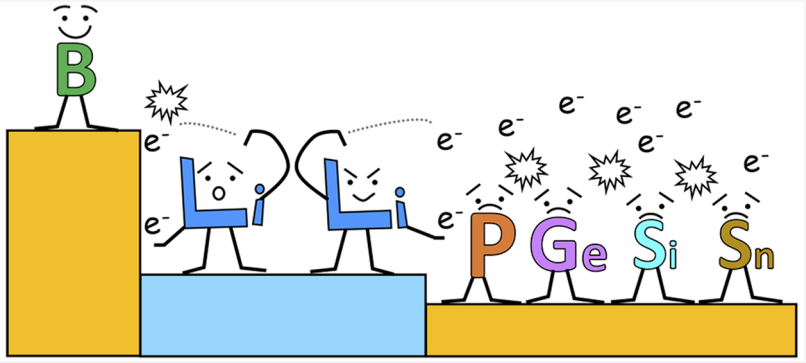

ABSTRACT: **Reduction or oxidation of a solid electrolyte (SE) by the electrodes of a battery can inject electrons or holes into the SE, inducing unwanted electrical conductivity and/or precipitating harmful interfacial reactions. Here, the likelihood for charge injection from a Li metal anode to 10 sulfide-based SEs is determined by computing the positions of the SE's band edges with respect to the electrochemical potential of the electrode. Although these SEs exhibit large band gaps (>4 eV), nearly all are susceptible to electron injection. One notable exception is the B-containing sulfide Li_3BS_3, which exhibits the greatest resistance to reduction. The trends in charge transfer stability are compared to those for chemical stability with a Li anode and are found to be similar. The combined characterization of chemical and charge transfer phenomena allows for a comprehensive assessment of interfacial stability. The utility of this approach is demonstrated by interpreting recent experiments on the $Li/Li_2H_2PO_4$/LGPS interface system.**

The global stock of electrified vehicles (EVs) is rising rapidly, having exceeded 7.2 million in 2019, and with potentially 140 million EVs predicted to be in use by 2030.[1] This increase has been enabled by the advent of Li-ion batteries. While Li-ion batteries exhibit the best combination of energy density, rechargeability, and cost of any commercialized battery chemistry, additional improvements in performance are highly desirable. One potential mechanism for improving performance is to replace commonly used flammable and volatile liquid electrolytes with a safer solid electrolyte (SE).[2] In addition, a SE can potentially enable the use of higher capacity negative electrodes, such as Li metal (3860 mAh/g vs 372 mAh/g for graphite).[3,4] Metal anodes are also an important component in advanced battery concepts that utilize sulfur or air cathodes.[5]

Among the various SEs, sulfides are noteworthy because of their high ionic conductivities, low grain-boundary resistance, and favorable mechanical properties.[6,7] An additional desirable feature for SEs is the ability to resist charge injection from the electrodes.[8] A viable SE should efficiently shuttle ions between electrodes, yet block electrons/holes from doing the same (which would result in self-discharge and/or short-circuiting).[9] The electrically insulating nature of a SE is often described in terms of a SE's band gap.[10] However, a description based on the bandgap alone is insufficient; rather the positions of the band edges—i.e., the conduction band minimum (CBM) and valence band maximum (VBM)—with respect to the electrochemical potentials of the electrodes that determines the tendency of a SE to undergo charge injection/extraction.

Figure 1a illustrates the relative energy levels of electrons in a battery's electrodes and in a SE.[8] If the CBM is higher in energy than the electrochemical potential of the anode (e.g.,

Received: November 11, 2020
Accepted: December 7, 2020
Published: December 14, 2020

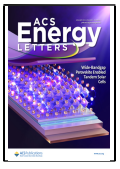

https://dx.doi.org/10.1021/acsenergylett.0c02372
ACS Energy Lett. 2021, 6, 150–157

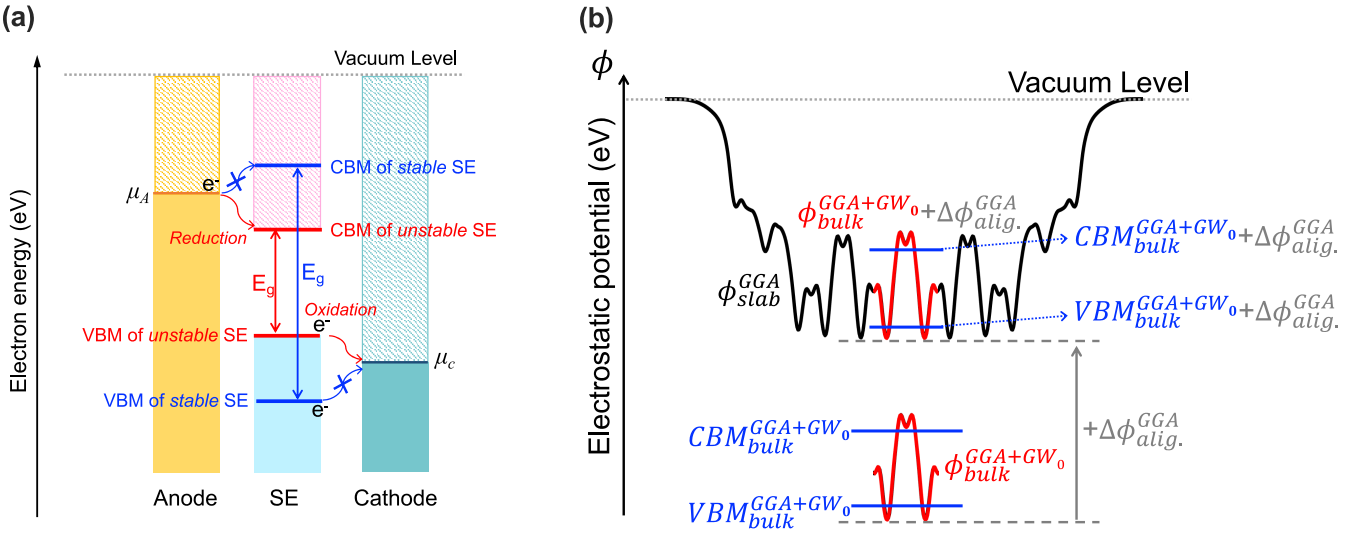

Figure 1. (a) Electron energy levels in solid electrolytes and electrodes. Cross-hatched (filled) areas represent empty (occupied) electron states. Blue and red lines depict the band edge positions for SEs that are stable and unstable, respectively. (b) Band edge alignment procedure for calculating the positions of the CBM and VBM. Black and red corrugations represent the planar-averaged electrostatic potentials for a surface slab and for the bulk, respectively. The gray arrow depicts the potential shift needed to align the electrostatic potentials of the bulk cell to the bulk region in the surface slab.

the Li/Li^+ level, $\mu_A = -1.39$ eV vs vacuum),[11] then no thermodynamic driving force exists for electron injection from the anode into the SE, i.e., a Schottky barrier exists.[12] Conversely, if the position of the CBM and μ_A are reversed, then reduction of the SE by the anode will be spontaneous. Similarly, at the interface with the cathode, if the VBM of the SE is lower in energy than the electrochemical potential of cathode (e.g., μ_C), hole injection into the SE resulting from electron injection in the cathode from the electrolyte is thermodynamically unfavored. If the ordering of these levels is reversed, then the cathode can oxidize the electrolyte, creating holes in the SE. These charge injection processes—electron insertion into the SE conduction band, or hole injection into the valence band—can stimulate self-discharge or short circuiting of the battery by introducing electronic charge carriers into the SE. Thus, the position of a SE's band edges, relative to the electrochemical potentials of the electrodes, is important for predicting the performance and stability of a solid electrolyte. Similar considerations apply to polaronic energy levels in the SE if the charge transferred to/from the electrolyte is localized. In summary, knowledge of a SE's bandgap alone is insufficient to predict a SE's tendency to undergo charge-transfer-related failure modes.

Another important feature of SEs is their chemical stability as a function of potential. The chemical stability window is the potential range for which the SE and electrode materials are more stable than any combination of competing phases formed from chemical (decomposition) reactions involving the SE and/or electrodes. Chemical stability can be calculated from the Li grand potential phase diagram.[13]

The concepts of charge transfer and chemical stability are complementary. For example, the electron transfer reactions described in the preceding discussion may constitute an initial step in a more extensive reaction cascade resulting in decomposition of the SE in the interfacial region. On the other hand, chemical decomposition often involves significant mass transfer and may be limited by slow kinetics. Given that electron transfer reactions can be rapid, the electronic charge transfer reactions may, in some cases, dominate over chemical reactions. Finally, even in cases where chemical decomposition does occur, charge transfer through an electronically insulating product phase may still occur via tunneling if the interphase is thin. Therefore, a more complete understanding of SE stability can be achieved by considering both charge transfer and chemical stability.[8,9,14] To date, few studies have characterized the tendency for charge transfer between metal anodes and SEs.[15−17]

The present study aims to predict the interfacial charge transfer stability between sulfide SEs and Li metal anodes. This is accomplished by predicting the absolute positions of the band edges of the SEs and electrode using state-of-the-art first-principles calculations. Bandgaps and absolute band edge positions of 10 SEs were evaluated using many-body perturbation theory.[18−20] Band edge positions were compared to the Li/Li^+ electrochemical potential to predict the propensity for reduction of a given SE by a Li metal anode.[15,21]

Although the SEs examined exhibit bandgaps larger than 4 eV, all but one are predicted to be susceptible to electron injection from Li metal, which is consistent with prior studies on several of these compounds. For comparison, the chemical interfacial stability with respect to Li was also evaluated as a function of potential and was found to closely follow the trends observed for charge transfer stability.[22,23] The combination of chemical and electochemical schemes allows for a thorough assessment of interfacial stability. Out of the SEs examined, Li_3BS_3 is predicted to exhibit the greatest resistance to reduction, with the CBM of the (100) facet of Li_3BS_3 predicted to be higher in energy than the Li/Li^+ level. These results suggest that B-containing sulfides hold more promise as SEs (relative to the other sulfides) in terms of their interfacial stability.

Finally, charge transfer stability is discussed in the context of interfacial coatings placed between the Li anode and a reactive SE. Taking the $Li/LiH_2PO_4/Li_{10}GeP_2S_{12}$ (LGPS)[24] system as an example, it is shown that an LiH_2PO_4 interlayer can block

https://dx.doi.org/10.1021/acsenergylett.0c02372
ACS Energy Lett. 2021, 6, 150−157

charge injection to the SE, potentially explaining the high interfacial stability achieved when LiH_2PO_4 is employed.

The position of the SE band edges, with respect to the vacuum level, can be determined by aligning the electrostatic potentials of a vacuum-slab supercell and that of a bulk cell (see Figure 1b). Here, ϕ_{slab}^{GGA} represents the planar-averaged electrostatic potential of a SE slab evaluated within the generalized gradient approximation (GGA). If the slab is of sufficient thickness, the electrostatic potential within the central region of the slab will have the same spatial dependence as in the bulk, $\phi_{bulk}^{GGA+GW_0}$, as determined by GW_0 calculations. (Because the electronic orbitals used in the GW_0 calculations are based on a prior bulk GGA calculation, the bulk electrostatic potential predicted by the GW_0 method is compatible with that of the slab calculation.) The bulk electrostatic potential is aligned with that of the bulk region of the slab by adding the alignment energy ($\Delta\phi_{alig}^{GGA}$). Finally, adding the alignment energy to the bulk CBM and VBM level (calculated by GGA+GW_0) yields the positions of the band edges referenced to the vacuum level, as summarized in the following equations:

$$\Delta\phi_{alig}^{GGA} = \phi_{slab}^{GGA}\Big|_{bulk\ region} - \phi_{bulk}^{GGA+GW_0} \quad (1)$$

$$VBM_{bulk}^{GGW+GW_0}|_{wrt\ VAC} = VBM_{bulk}^{GGW+GW_0} + \Delta\phi_{alig}^{GGA} \quad (2)$$

$$CBM_{bulk}^{GGW+GW_0}|_{wrt\ VAC} = CBM_{bulk}^{GGW+GW_0} + \Delta\phi_{alig}^{GGA} \quad (3)$$

Table 1 summarizes the calculated bandgaps of the 10 SEs examined in the present study. These values were determined using the GW_0 method with input wave functions determined from a preceding Perdew−Burke−Ernzerhof (PBE)-based calculation. A comparison of band gaps calculated with different variants of the GW method (G_0W_0 or GW) and input wave functions is presented in Table S1 in the Supporting Information. The combination of PBE wave functions with the GW_0 method was adopted here, because of its ability to predict the absolute positions of band edges in semiconductor materials with low error.[28]

Table 1. SE Band Gaps Calculated Using the GW_0 Method

solid electrolyte	band gap (eV)
$Li_{10}GeP_2S_{12}$ (LGPS)	4.09
$Li_{10}SnP_2S_{12}$	4.02
$Li_{10}SiP_2S_{12}$	4.28
γ-Li_3PS_4	4.82
β-Li_3PS_4	5.04
Li_4GeS_4	4.50
Li_4SnS_4	4.03
Li_3BS_3	5.03
$Li_2B_2S_5$	4.24
Li_2S	5.52

All of the SEs examined exhibit bandgaps greater than 4 eV. These relatively large gaps imply that the intrinsic compositions of these materials are likely to be electronic insulators, with respect to thermal excitation of carriers. The SE containing BS_3 or PS_4 complex anions, such as Li_3BS_3 and β-Li_3PS_4, exhibit the largest bandgaps, approaching 5 eV. As expected, the polymorphs of Li_3PS_4 (β- and γ-), both of which contain tetrahedral PS_4^{3-} anions, have similar band gaps, differing by only ∼0.2 eV. On the other hand, the chemically similar compounds $Li_2B_2S_5$ and Li_3BS_3 exhibit band gaps that differ by 0.6 eV. This difference may arise from differences in the composition and charge state of their respective complex anions: in Li_3BS_3 the anion units are comprised of BS_3^{3-} clusters, while $Li_2B_2S_5$ is based on $B_2S_5^{2-}$ anions. Another noteworthy observation applies to the Sn-containing compounds, $Li_{10}SnP_2S_{12}$ and Li_4SnS_4. These SE exhibit almost-identical band gaps of 4.02 and 4.03 eV, respectively, which are the smallest among the SEs exmained here. Hence, the addition of P to Li_4SnS_4 to form $Li_{10}SnP_2S_{12}$ does not change the band gap. This insensitivity to P addition can be traced the orbital nature of the band edges of $Li_{10}SnP_2S_{12}$. The density of states (DOS) plot in Figure S1(a) in the Supporting Information shows that, in $Li_{10}SnP_2S_{12}$, both the VBM and CBM are derived primarily from S orbitals, with much less weight from P orbitals. This behavior is consistent with marginal changes in the bandgap upon P addition. This behavior differs from that of Li_4GeS_4/LGPS, where the addition of P decreases the band gap by nearly 0.5 eV: 4.50 eV (Li_4GeS_4) → 4.09 eV (LGPS). The calculated density of states (DOS) in Figure S1(b) in the Supporting Information suggests that the sensitivity of the bandgap to P introduction may be due to the nearly equal weight of P and Ge orbitals to the CBM in LGPS.

Figure 2a illustrates the band-edge positions of SEs, with respect to Li/Li^+. Red and blue bars represent the conduction and valence bands for the lowest energy surface facets, respectively. With the exception of Li_2S, which is not a superionic conductor, all of the SEs examined here have CBM that are lower in energy than the electrochemical potential of Li metal. Hence, based on thermodynamics, all are expected to undergo electron injection from (i.e., be reduced by) a Li anode. This conclusion holds, regardless of whether the electrons are added to the SE reside in the conduction band, or form new, localized states. The latter polarnic states will be positioned below the CBM, and would thus exert an even stronger driving force for electron transfer from the anode.

In the case of the $Li_{10}XP_2S_{12}$ family, where X = Sn, Ge, and Si, all compositions have CBMs that are significantly lower in energy (∼1.3−2.3 eV) than the Li/Li^+ level. This behavior implies that a strong energetic driving force exists for the reduction of these SE by Li, in agreement with experiments.[25] Furthermore, the positions of CBM of LGPS and $Li_{10}SnP_2S_{12}$ are similar, implying that substituting Sn for Ge does not change the electronic structure significantly. In contrast, substituting Si for Ge in LGPS has a greater impact on the electronic structure−Si substitution increases the CBM position of LGPS by ∼1 eV.

In the case of the LPS family, γ- and β-Li_3PS_4, the CBM positions fall below the Li electrochemical potential by 1.41 and 1.25 eV, respectively, which is similar to the behavior of the $Li_{10}XP_2S_{12}$ family. Consequently, a large driving force for charge injection exists. Varying the orientation of the surface (through which charge transfer occurs) alters the CBM position by ∼1 eV, but these changes are not sufficient to raise the CBM above the Li/Li^+ level.

The slightly higher positions of the CBM in Li_4GeS_4 and Li_4SnS_4 imply that these SE are marginally more stable than are the LPS polymorphs—yet still unstable in an absolute sense against charge injection. This behavior holds even though their respective band gaps are smaller than those of the LPS polymorphs; this observation further highlights the greater

https://dx.doi.org/10.1021/acsenergylett.0c02372
ACS Energy Lett. 2021, 6, 150−157

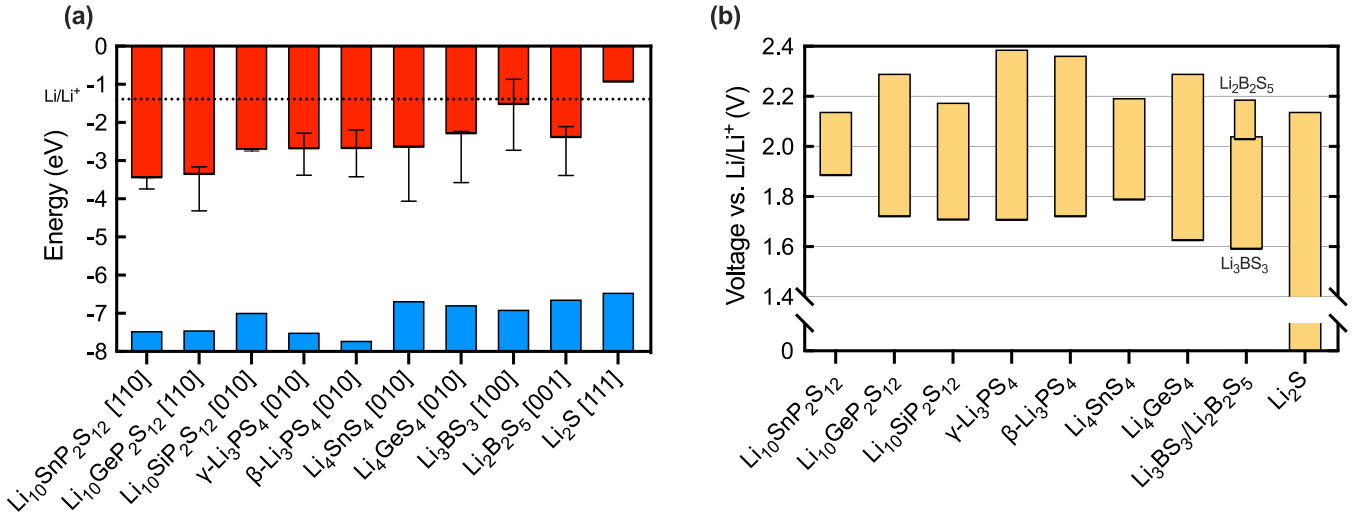

Figure 2. (a) Calculated band edge positions of SEs. Red and blue bars represent the conduction and valence bands, respectively, for the lowest energy surface facets (identified on the *x*-axis). Error bars represent the range of variations in the CBM due to changes in the orientation and/or composition of the surface slab used in the calculation. The vacuum level is assigned a value of zero; the Li/Li^+ level is represented with a dotted line. (b) Chemical stability window of SEs as a function of composition.

importance of the band edge positions, relative to band gaps in determining stability against electronic charge transfer.

The Li−B−S containing solid electrolytes, $Li_2B_2S_5$ and Li_3BS_3, are predicted to be somewhat more resistant to electron injection. These compositions are based on $B_2S_5^{2-}$ and BS_3^{3-} complex anions, respectively, which differ in structure from the S-based tetrahedral anions (XS_4) present in all of the preceding systems. In the case of $Li_2B_2S_5$, the CBM for the (001)-oriented surface is ∼1 eV lower than the Li electrochemical potential. While this represents improved stability against charge injection, compared to the previously discussed SEs, a relatively strong driving force for reduction still exists. This instability also applies to the other facets of $Li_2B_2S_5$.

In contrast, Li_3BS_3 is predicted to exhibit the best stability against undesirable charge transfer out of all of the SE examined. For the lowest energy (100) facet of Li_3BS_3 (surface energy of 0.37 J/m^2), the CBM is lower than Li/Li^+ level by only 0.2 eV, which is the smallest among the SEs examined. The highest energy (001) facet (surface energy of 0.54 J/m^2) is more prone to charge injection: its CBM is positioned 1.4 eV lower than the Li/Li^+ level. This trend is reversed for the (010) facet (surface energy of 0.44 J/m^2), whose CBM is 0.5 eV *higher* than Li/Li^+, corresponding to the upper error bar in Figure 2a. In this case, charge transfer from Li metal to SE is thermodynamically unfavorable. Figure S2 in the Supporting Information illustrates the equilibrium crystallite shape for Li_3BS_3 and shows that the stable intermediate-energy (010) facet comprises a sizable fraction of the crystalite area. A recent study based on ab initio molecular dynamics (MD)[26] claimed that $Li_2B_2S_5$ and Li_3BS_3 exhibit high ionic conductivities of 9.7 and 2 mS/cm, respectively, at room temperature. Nudged elastic band calculations of the Li migration barrier in Li_3BS_3 found values less than 0.25 eV.[27] The present analysis also suggests that Li_3BS_3 exhibits promising stability, with respect to charge injection from Li. Taken together, these data suggest that Li_3BS_3 may be a SE whose performance warrants additional experimental scrutiny.

Although not a fast Li-ion conductor, for reference, the band-edge positions of Li_2S are also plotted in Figure 2. Consistent with experimental data suggesting that Li_2S is not reduced by Li metal,[25] the CBM of Li_2S is predicted to be positioned at higher energies than the Li/Li^+ level.

Regarding the resistance of the SE to oxidation by a cathode, it is noteworthy that the VBM all of the SE examined here (shown as blue bars in Figure 2a) are positioned at very low energies, relative to the Li electrochemical potential: generally, the VBM are 5.2−6.4 eV lower in energy (or, equivalently, 5.2−6.4 V more positive in potential) than Li/Li^+. Typical Li-ion battery cathodes operate in the range of 3.5−4.2 V vs Li/Li^+.[28] The average positions of the VBM for the sulfide SE examined here are 2.2 and 1.5 eV lower in energy, respectively, than the corresponding electrochemical potentials of 3.5 and 4.2 V cathodes. Hence, these SEs are predicted to be resistant to charge extraction by commonly used cathode materials.

Figure 2b shows the chemical stability windows of the SEs, as a function of cell voltage. The SEs are predicted to be stable against decomposition and/or reaction with a Li metal anode for the voltage ranges spanned by the yellow bars. The windows for some of the SEs examined here ($Li_{10}SnP_2S_{12}$, LGPS, $Li_{10}SiP_2S_{12}$, Li_3PS_4 polymorphs, Li_4GeS_4, and Li_2S) have been reported elsewhere,[29] and the present results are similar to prior studies. However, to our knowledge, the stabilty windows of the B-based SEs and for Li_4SnS_4 have not been reported.

Regarding chemical stability with respect to reduction by a Li anode, all of the SE examined here are predicted to react/decompose at voltages of <1.9 V (at worst) to 1.6 V (at best), with respect to Li/Li^+. Li_2S is predicted to be the only compound that is stable at 0 V; however, as discussed above, it is not a superionic conductor. The poor chemical stability of the sulfides against Li roughly mimics the trends in resistance to charge injection. For example, the chemical (Figure 2b) and charge transfer (Figure 2a) stabilities of Li_3BS_3 and Li_4GeS_4 predicted by both metrics suggest that these are the two most stable SEs (against a Li anode). In a similar vein, $Li_{10}SnP_2S_{12}$ is predicted by both metrics to be the least stable. On average, the sulfides examined here are predicted to undergo reductive charge transfer from Li for electrode potentials less than 1.12

https://dx.doi.org/10.1021/acsenergylett.0c02372
ACS Energy Lett. 2021, 6, 150−157

(± 0.8) V vs Li/Li$^+$. This value is roughly similar to the average chemical stability limit for reduction (1.76 (± 0.7) V).

Although the charge transfer stability of $Li_{10}SnP_2S_{12}$ and $Li_{10}GeP_2S_{12}$ are similar, differences in their chemical composition can influence which phases form, should these SE chemically decompose. These decomposition products could be more or less stable (again, depending on the composition), and these differences in phase stability will impact their overall chemical stabilities. Hence, it is possible that compounds having similar band-edge positions (and, thus, similar charge-transfer stability) may still exhibit different chemical stabilities, although, as shown here, the overall trends between the two stability types are similar.

More broadly, none of the SE examined here are predicted to be chemically stable at high voltages. At best, in the case of γ-Li_3PS_4, these compounds are stable up to ~2.4 V; at worst, in the case of LGPS, stability is maintained only up to ~2.1 V. Overall, the maximum range of the chemical stability window (the voltage range over which a SE is resistant to both oxidation and reduction reactions) of the surfide SE examined here is very narrow, spanning only from 1.6 V to 2.4 V. Moreover, the trends in oxidative stability for the sulfides differ qualitatively from their stability against charge extraction; however, none of the SE examined here are chemically stable against a typical high-voltage cathode (Figure 2b), and all are predicted to be stable, with respect to electron extraction (Figure 2a). This suggests that chemical oxidative stability with the cathode is the primary limiting factor for these SEs (assuming the kinetics of these reactions are not sluggish).

Given the poor stability of the sulfide SE at low potentials, several studies have investigated the use of coatings (positioned between the SE and Li electrode) to prevent these SE from reacting with Li.[24,30−35] For example, $Li_2H_2PO_4$ (LHPO) has been proposed as a coating between Li and LGPS.[24] Li grand potential phase diagram calculations predict that LHPO should decompose to form Li_2O, Li_3P, and LiH when it directly contacts Li metal.[36] Nevertheless, decomposition of LHPO was not observed in experiments, and, concomitantly, the interfacial resistance decreased and the cycling performance improved, in comparison to the cell where LHPO an coating was not used.[24]

Figure 3 illustrates the positions of the Li/Li$^+$ electrochemical potential, and the calculated positions of the CBMs

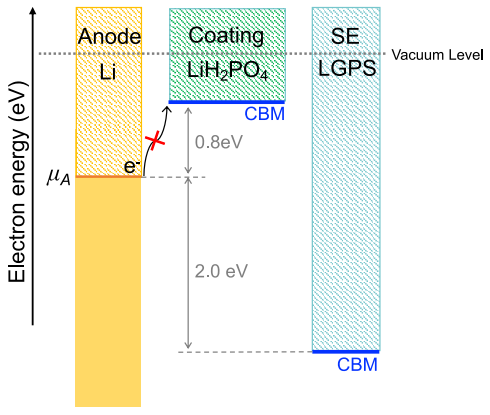

Figure 3. Positions of the electrochemical potential of a Li anode (μ_A), the CBM of a LHPO coating, and the CBM of a LGPS SE. The hatched areas represent unfilled electron states. The energy gaps between μ_A and the CBM are indicated.

of LHPO and LGPS. These calculations reveal that the Li/Li$^+$ level is 0.8 eV lower in energy than is the CBM of LHPO. Thus, electron transfer from Li to LHPO is energetically unfavorable. By acting as an intervening barrier to electron transfer, LHPO can suppress the reduction of LGPS, whose CBM is ~2 eV lower in energy than the Li electrochemical potential.

Taken together, these observations suggest that the good performance observed for the Li/LHPO/LGPS system experimentally[24] derived from a combination of (a) slow mass transport, which kinetically hinders the tendency for LHPO to chemically react at low voltages,[36] and (b) the high energy of the LHPO CBM, which hinders change transfer from the anode, and ultimately into LGPS. To achieve a complete understanding of the stability of this interfacial system, it is desirable to consider both chemical and charge-transfer stability, as demonstrated here.

In closing, the reduction or oxidation of a solid electrolyte (SE) by the electrodes of a battery can induce unwanted electrical conductivity and/or precipitate harmful interfacial reactions. The present study has evaluated the likelihood for charge injection from a Li metal anode to 10 sulfide-based SEs by computing the positions of the SE's band edges with respect to the electrochemical potential of the electrode. Although these SEs exhibit large band gaps (>4 eV), nearly all are susceptible to electron injection; the greatest resistance to reduction is exhibited by the B-containing sulfide Li_3BS_3. Notably, the trends in charge-transfer stability from a Li anode to the SE are similar to those for interfacial *chemical* stability.

Trends in oxidative stability for the sulfides differ qualitatively from their stability against charge extraction: while none of the SE examined here are chemically stable against high-voltage cathodes, all are predicted to be stable with respect to electron extraction. Assuming that chemical kinetics are not slow, this suggests that chemical oxidative stability with the cathode is the primary limiting factor for these SEs.

The combined characterization of chemical and charge transfer phenomena allows for a thorough assessment of interfacial stability. As an example of this approach, an analysis based on band-edge positions is used to clarify the role of coatings that have been reported to stabilize the interface between Li and LGPS. In particular, the improvements in performance in the presence of an LHPO interlayer are attributed to favorable band-edge alignment. Although LGPS has a low CBM and is thus susceptible to electron transfer from Li, an intervening layer of LHPO can block this charge transfer because its CBM is higher in energy than the Li electrochemical potential. Thus, charge injection into SEs can be prevented by identifying interlayer coatings having CBMs with high energies.

METHODS

Bandgaps and the positions of the conduction and valence band edges of 10 model SSEs (LGPS, $Li_{10}SnP_2S_{12}$, $Li_{10}SiP_2S_{12}$, β- and γ-Li_3PS_4, Li_4GeS_4, Li_4SnS_4, Li_3BS_3, $Li_2B_2S_5$, and Li_2S) were evaluated using DFT[37] and quasi-particle methods,[18−20] as implemented in the Vienna Ab initio Simulation Package.[38] The semilocal PBE-GGA[39] or the HSE06 hybrid functional[40,41] were used to predict structural properties and input wave functions for subsequent GW-based calculations. The planewave cutoff energy was set as follows: 300 eV for LGPS, $Li_{10}SnP_2S_{12}$, $Li_{10}SiP_2S_{12}$, β- and γ-Li_3PS_4, Li_4GeS_4, and

https://dx.doi.org/10.1021/acsenergylett.0c02372
ACS Energy Lett. 2021, 6, 150−157

Li_4SnS_4; 350 eV for Li_3BS_3 and $Li_2B_2S_5$; and 450 eV for Li_2S. Γ-centered *k*-point sampling grids were used in combination with the following *k*-point grid densities: 2 × 2 × 1 (for LGPS, $Li_{10}SnP_2S_{12}$, $Li_{10}SiP_2S_{12}$, Li_4GeS_4, and Li_4SnS_4); 2 × 2 × 2 (for γ-Li_3PS_4, Li_3BS_3, and $Li_2B_2S_5$); 3 × 3 × 3 (for β-Li_3PS_4); and 4 × 4 × 4 (for Li_2S).

Li lattice sites in LGPS are partially occupied. Supercell models accounting for this partial occupancy were constructed using *pymatgen*.[22,23] Five hundred (500) structural candidates for LGPS were generated, consistent with the prescribed stoichiometry. The internal degrees of freedom for these structures were relaxed to a force tolerance of 0.01 eV/Å. The most stable structure (having lowest total energy) was identified. Figure S3 in the Supporting Information shows the energy per atom of the 500 candidate structures. The lowest energy structure agrees with that reported in a recent DFT study;[42] in this structure, the edges of LiS_6 polyhedra are shared by Ge or P. The 14 Li atoms present in the cell are located in four channels, with three or four ions per channel. Figure S4(a) in the Supporting Information illustrates the Li atom distribution in these channels (which are oriented along the *z*-direction). Unfortunately, the presence of Li partial occupancies complicates the construction of vacuum slabs that have identical compositions on both surfaces (see Figure S4(a)). Surfaces having different compositions will result in the formation of an undesirable dipole within the simulation cell. Furthermore, identical surface compositions are needed to unambiguously identify the band-edge positions. Symmetric surface slabs were constructed by arranging the Li atoms within the bulk conducting channels symmetrically, with respect to (010) and (110) planes (Figure S4(b) in the Supporting Information). The total energy of this symmetrized bulk structure (shown as a red line in Figure S3) is 2 meV/atom higher than that of the lowest energy structure identified.

Crystal structures for $Li_{10}MP_2S_{12}$ (M = Sn, Si) were generarted by substituting for Ge in LGPS with Sn or Si.[10] Equilibrium cell volumes were determined by fitting volume-energy data to the Murnaghan equation of state,[43] while relaxing the atom positions to a force tolerance of 0.01 eV/Å.

DFT-GGA, hybrid functionals, and GW methods[18−20] were used to predict the bandgaps of SEs. Table S1 in the Supporting Information summarizes the calculated bandgaps, as a function of the calculation method. Among the several GW variants, the PBE+GW_0 variant[44] was adopted, because of its ability to accurately reproduce experimental band offsets.[45] A large number of empty bands were used in the calculations to accurately predict the band-edge positions:[46] Four thousand four hundred (4400) bands were used for LGPS, $Li_{10}SnP_2S_{12}$, $Li_{10}SiP_2S_{12}$, 4200 for Li_3BS_3, $Li_2B_2S_5$, 4000 for β-Li_3PS_4, 3360 for γ-Li_3PS_4, Li_4GeS_4, Li_4SnS_4, and 528 for Li_2S. These values were determined by running a series of PBE+G_0W_0 calculations and incrementally increasing the number of bands until the band gap and band edges converged to within 0.02−0.03 meV/band. Using this same convergence criterion, the number of frequency points was set to 50.

The identification of low-energy surfaces of the SE is required for establishing band-edge positions. Surface energies were calculated for the following SE/surface normal combinations: LGPS ([010], [110]), $Li_{10}SnP_2S_{12}$ ([010], [110]), $Li_{10}SiP_2S_{12}$ ([010], [110]), β-Li_3PS_4 ([100], [010], [001]), γ-Li_3PS_4 ([100], [010]), Li_4GeS_4 ([100], [010]), Li_4SnS_4 ([100], [010]), $Li_2B_2S_5$ ([100], [001], [110]), Li_3BS_3 ([001], [010], [100]), and Li_2S ([111]). The low energy surface of Li_2S was adopted from our previous work.[47] The surface energies were calculated as a function of the Li chemical potential. The chemical potential of Li (μ_{Li}) in a SE in contact with Li metal is assumed to be set by the energy per atom in bulk BCC Li (μ_{Li}(BCC Li)), i.e., equilibrium with Li metal is assumed.[48] The surface energies (γ_{SE}) can be expressed as

$$\gamma_{SE}(\mu_{Li}) = E_{slab} - n_{Li}\mu_{Li} - \sum_i n_i\mu_i \quad (4)$$

where E_{slab} is the total energy surface slab, n_i is the number of atoms of type *i* in the slab (excluding Li), and μ_i is the corresponding chemical potential. The chemical potentials of the non-Li elements were evaluated assuming that each SE was in equilibrium with their competing phases (see the Supporting Information for additional details). Because of their structural similarities, the surfaces of $Li_{10}SnP_2S_{12}$ and $Li_{10}SiP_2S_{12}$ adopted the same structure as the [010] and [110] surfaces of LGPS. The lowest-energy surface for each compound was used to evaluate its band-edge positions.

■ ASSOCIATED CONTENT

Supporting Information

The Supporting Information is available free of charge at https://pubs.acs.org/doi/10.1021/acsenergylett.0c02372.

Bandgaps of SEs calculated by various GW methods; partial density of states plots for $Li_{10}SnP_2S_{12}$ and LGPS; equilibrium crystallite shape for Li_3BS_3; energies of candidate LGPS structures; distribution of Li atoms in LGPS; equations determining the chemical potentials of each species in the various sulfide SE (PDF)

■ AUTHOR INFORMATION

Corresponding Author

Donald J. Siegel − *Mechanical Engineering Department, Materials Science & Engineering, Applied Physics Program, University of Michigan Energy Institute, and Joint Center for Energy Storage Research, University of Michigan, Ann Arbor, Michigan 48109-2125, United States;* orcid.org/0000-0001-7913-2513; Phone: +1 (734) 764-4808; Email: djsiege@umich.edu

Authors

Haesun Park − *Mechanical Engineering Department, University of Michigan, Ann Arbor, Michigan 48109-2125, United States;* orcid.org/0000-0001-6266-8151

Seungho Yu − *Center for Energy Storage Research, Korea Institute of Science and Technology (KIST), Seongbuk-gu, Seoul 02792, Republic of Korea;* orcid.org/0000-0003-3912-6463

Complete contact information is available at: https://pubs.acs.org/10.1021/acsenergylett.0c02372

Notes

The authors declare no competing financial interest.

■ ACKNOWLEDGMENTS

This work was supported as part of the Joint Center for Energy Storage Research (JCESR), an Energy Innovation Hub funded by the U.S. Department of Energy, Office of Science, and Basic Energy Sciences. S.Y. was supported by the institutional

program of the Korea Institute of Science and Technology (Project No. 2E30202).

REFERENCES

(1) *Global EV Outlook 2020 Entering the decade of electric drive?*; International Energy Agency, 2020.

(2) Zhang, Z.; Shao, Y.; Lotsch, B.; Hu, Y.-S.; Li, H.; Janek, J.; Nazar, L. F.; Nan, C.-W.; Maier, J.; Armand, M.; Chen, L. New horizons for inorganic solid state ion conductors. *Energy Environ. Sci.* **2018**, *11*, 1945−1976.

(3) Chandrashekar, S.; Trease, N. M.; Chang, H. J.; Du, L.-S.; Grey, C. P.; Jerschow, A. ^{7}Li MRI of Li batteries reveals location of microstructural lithium. *Nat. Mater.* **2012**, *11*, 311−311.

(4) Xu, W.; Wang, J.; Ding, F.; Chen, X.; Nasybulin, E.; Zhang, Y.; Zhang, J.-G. Lithium metal anodes for rechargeable batteries. *Energy Environ. Sci.* **2014**, *7*, 513−537.

(5) Zhou, L.; Assoud, A.; Zhang, Q.; Wu, X.; Nazar, L. F. New Family of Argyrodite Thioantimonate Lithium Superionic Conductors. *J. Am. Chem. Soc.* **2019**, *141*, 19002−19013.

(6) Manthiram, A.; Yu, X.; Wang, S. Lithium battery chemistries enabled by solid-state electrolytes. *Nat. Rev. Mater.* **2017**, *2*, 16103.

(7) Chen, S.; Xie, D.; Liu, G.; Mwizerwa, J. P.; Zhang, Q.; Zhao, Y.; Xu, X.; Yao, X. Sulfide solid electrolytes for all-solid-state lithium batteries: Structure, conductivity, stability and application. *Energy Storage Mater.* **2018**, *14*, 58−74.

(8) Goodenough, J. B.; Kim, Y. Challenges for rechargeable Li batteries. *Chem. Mater.* **2010**, *22*, 587−603.

(9) Goodenough, J. B.; Park, K.-S. The Li-Ion Rechargeable Battery: A Perspective. *J. Am. Chem. Soc.* **2013**, *135*, 1167−1176.

(10) Ong, S. P.; Mo, Y.; Richards, W. D.; Miara, L.; Lee, H. S.; Ceder, G. Phase stability, electrochemical stability and ionic conductivity of the $Li_{10\pm1}MP_2X_{12}$ (M = Ge, Si, Sn, Al or P, and X = O, S or Se) family of superionic conductors. *Energy Environ. Sci.* **2013**, *6*, 148−156.

(11) The absolute electrode potential: an explanatory note (Recommendations 1986). *J. Electroanal. Chem. Interfacial Electrochem.* **1986**, *209*, 417−428.

(12) Mishra, U. K.; Singh, J. *Semiconductor Device Physics and Design*; Springer: Dordrecht, The Netherlands, 2007.

(13) Nolan, A. M.; Zhu, Y.; He, X.; Bai, Q.; Mo, Y. Computation-Accelerated Design of Materials and Interfaces for All-Solid-State Lithium-Ion Batteries. *Joule* **2018**, *2*, 2016−2046.

(14) Peljo, P.; Girault, H. H. Electrochemical potential window of battery electrolytes: the HOMO−LUMO misconception. *Energy Environ. Sci.* **2018**, *11*, 2306−2309.

(15) Thompson, T.; Yu, S.; Williams, L.; Schmidt, R. D.; Garcia-Mendez, R.; Wolfenstine, J.; Allen, J. L.; Kioupakis, E.; Siegel, D. J.; Sakamoto, J. Electrochemical Window of the Li-Ion Solid Electrolyte $Li_7La_3Zr_2O_{12}$. *ACS Energy Lett.* **2017**, *2*, 462−468.

(16) Kim, K.; Siegel, D. J. Predicting Wettability and the Electrochemical Window of Lithium-Metal/Solid Electrolyte Interfaces. *ACS Appl. Mater. Interfaces* **2019**, *11*, 39940−39950.

(17) Song, W.; Scholtis, E. S.; Sherrell, P. C.; Tsang, D. K. H.; Ngiam, J.; Lischner, J.; Fearn, S.; Bemmer, V.; Mattevi, C.; Klein, N.; Xie, F.; Riley, D. J. Electronic structure influences on the formation of the solid electrolyte interphase. *Energy Environ. Sci.* **2020**, DOI: 10.1039/D0EE01825B.

(18) Hedin, L. New Method for Calculating the One-Particle Green's Function with Application to the Electron-Gas Problem. *Phys. Rev.* **1965**, *139*, A796−A823.

(19) Hybertsen, M. S.; Louie, S. G. Electron correlation in semiconductors and insulators: Band gaps and quasiparticle energies. *Phys. Rev. B: Condens. Matter Mater. Phys.* **1986**, *34*, 5390−5413.

(20) Shishkin, M.; Kresse, G. Implementation and performance of the frequency-dependent GW method within the PAW framework. *Phys. Rev. B: Condens. Matter Mater. Phys.* **2006**, *74*, 35101.

(21) Kumar, N.; Siegel, D. J. Interface-Induced Renormalization of Electrolyte Energy Levels in Magnesium Batteries. *J. Phys. Chem. Lett.* **2016**, *7*, 874−881.

(22) Ong, S. P.; Wang, L.; Kang, B.; Ceder, G. Li−Fe−P−O_2 Phase Diagram from First Principles Calculations. *Chem. Mater.* **2008**, *20*, 1798−1807.

(23) Ong, S. P.; Jain, A.; Hautier, G.; Kang, B.; Ceder, G. Thermal stabilities of delithiated olivine MPO_4 (M = Fe, Mn) cathodes investigated using first principles calculations. *Electrochem. Commun.* **2010**, *12*, 427−430.

(24) Zhang, Z.; Chen, S.; Yang, J.; Wang, J.; Yao, L.; Yao, X.; Cui, P.; Xu, X. Interface Re-Engineering of $Li_{10}GeP_2S_{12}$ Electrolyte and Lithium anode for All-Solid-State Lithium Batteries with Ultralong Cycle Life. *ACS Appl. Mater. Interfaces* **2018**, *10*, 2556−2565.

(25) Wenzel, S.; Randau, S.; Leichtweiß, T.; Weber, D. A.; Sann, J.; Zeier, W. G.; Janek, J. Direct Observation of the Interfacial Instability of the Fast Ionic Conductor $Li_{10}GeP_2S_{12}$ at the Lithium Metal Anode. *Chem. Mater.* **2016**, *28*, 2400−2407.

(26) Sendek, A. D.; Cubuk, E. D.; Antoniuk, E. R.; Cheon, G.; Cui, Y.; Reed, E. J. Machine Learning-Assisted Discovery of Solid Li-Ion Conducting Materials. *Chem. Mater.* **2019**, *31*, 342−352.

(27) Bianchini, F.; Fjellvåg, H.; Vajeeston, P. A first-principle investigation of the Li diffusion mechanism in the super-ionic conductor lithium orthothioborate Li_3BS_3 structure. *Mater. Lett.* **2018**, *219*, 186−189.

(28) Manthiram, A. A reflection on lithium-ion battery cathode chemistry. *Nat. Commun.* **2020**, *11*, 1550.

(29) Zhu, Y.; He, X.; Mo, Y. Origin of Outstanding Stability in the Lithium Solid Electrolyte Materials: Insights from Thermodynamic Analyses Based on First-Principles Calculations. *ACS Appl. Mater. Interfaces* **2015**, *7*, 23685−23693.

(30) Ogawa, M.; Kanda, R.; Yoshida, K.; Uemura, T.; Harada, K. High-capacity thin film lithium batteries with sulfide solid electrolytes. *J. Power Sources* **2012**, *205*, 487−490.

(31) Davis, A. L.; Garcia-Mendez, R.; Wood, K. N.; Kazyak, E.; Chen, K.-H.; Teeter, G.; Sakamoto, J.; Dasgupta, N. P. Electro-chemo-mechanical evolution of sulfide solid electrolyte/Li metal interfaces: operando analysis and ALD interlayer effects. *J. Mater. Chem. A* **2020**, *8*, 6291−6302.

(32) Wang, C.; Adair, K. R.; Liang, J.; Li, X.; Sun, Y.; Li, X.; Wang, J.; Sun, Q.; Zhao, F.; Lin, X.; Li, R.; Huang, H.; Zhang, L.; Yang, R.; Lu, S.; Sun, X. Solid-State Plastic Crystal Electrolytes: Effective Protection Interlayers for Sulfide-Based All-Solid-State Lithium Metal Batteries. *Adv. Funct. Mater.* **2019**, *29*, 1900392.

(33) Gao, Y.; Wang, D.; Li, Y. C.; Yu, Z.; Mallouk, T. E.; Wang, D. Salt-Based Organic−Inorganic Nanocomposites: Towards A Stable Lithium Metal/$Li_{10}GeP_2S_{12}$ Solid Electrolyte Interface. *Angew. Chem., Int. Ed.* **2018**, *57*, 13608−13612.

(34) Chien, P.-H.; Feng, X.; Tang, M.; Rosenberg, J. T.; O'Neill, S.; Zheng, J.; Grant, S. C.; Hu, Y.-Y. Li Distribution Heterogeneity in Solid Electrolyte $Li_{10}GeP_2S_{12}$ upon Electrochemical Cycling Probed by ^{7}Li MRI. *J. Phys. Chem. Lett.* **2018**, *9*, 1990−1998.

(35) Umeshbabu, E.; Zheng, B.; Zhu, J.; Wang, H.; Li, Y.; Yang, Y. Stable Cycling Lithium−Sulfur Solid Batteries with Enhanced Li/$Li_{10}GeP_2S_{12}$ Solid Electrolyte Interface Stability. *ACS Appl. Mater. Interfaces* **2019**, *11*, 18436−18447.

(36) Xiao, Y.; Miara, L. J.; Wang, Y.; Ceder, G. Computational Screening of Cathode Coatings for Solid-State Batteries. *Joule* **2019**, *3*, 1252−1275.

(37) Hohenberg, P.; Kohn, W. Inhomogeneous Electron Gas. *Phys. Rev.* **1964**, *136*, B864−B871.

(38) Kresse, G.; Furthmuller, J. Efficient iterative schemes for ab initio total-energy calculations using a plane-wave basis set. *Phys. Rev. B: Condens. Matter Mater. Phys.* **1996**, *54*, 11169−11186.

(39) Perdew, J. P.; Burke, K.; Ernzerhof, M. Generalized Gradient Approximation Made Simple. *Phys. Rev. Lett.* **1996**, *77*, 3865−3868.

(40) Heyd, J.; Scuseria, G. E. Efficient hybrid density functional calculations in solids: Assessment of the Heyd−Scuseria−Ernzerhof screened Coulomb hybrid functional. *J. Chem. Phys.* **2004**, *121*, 1187−1192.

(41) Krukau, A. V.; Vydrov, O. A.; Izmaylov, A. F.; Scuseria, G. E. Influence of the exchange screening parameter on the performance of screened hybrid functionals. *J. Chem. Phys.* **2006**, *125*, 224106.
(42) Oh, K.; Chang, D.; Lee, B.; Kim, D.-H.; Yoon, G.; Park, I.; Kim, B.; Kang, K. Native Defects in $Li_{10}GeP_2S_{12}$ and Their Effect on Lithium Diffusion. *Chem. Mater.* **2018**, *30*, 4995−5004.
(43) Murnaghan, F. D. The Compressibility of Media under Extreme Pressures. *Proc. Natl. Acad. Sci. U. S. A.* **1944**, *30*, 244−247.
(44) Shishkin, M.; Kresse, G. Self-consistent GW calculations for semiconductors and insulators. *Phys. Rev. B: Condens. Matter Mater. Phys.* **2007**, *75*, 235102−235102.
(45) Grüneis, A.; Kresse, G.; Hinuma, Y.; Oba, F. Ionization Potentials of Solids: The Importance of Vertex Corrections. *Phys. Rev. Lett.* **2014**, *112*, 96401.
(46) Shishkin, M.; Marsman, M.; Kresse, G. Accurate quasiparticle spectra from self-consistent GW calculations with vertex corrections. *Phys. Rev. Lett.* **2007**, *99*, 246403−246403.
(47) Park, H.; Koh, H. S.; Siegel, D. J. First-Principles Study of Redox End Members in Lithium−Sulfur Batteries. *J. Phys. Chem. C* **2015**, *119*, 4675−4683.
(48) Hummelshøj, J. S.; Luntz, A. C.; Nørskov, J. K. Theoretical evidence for low kinetic overpotentials in Li-O_2 electrochemistry. *J. Chem. Phys.* **2013**, *138*, 034703.

https://dx.doi.org/10.1021/acsenergylett.0c02372
ACS Energy Lett. 2021, 6, 150−157